Non-modal hydrodynamic stability analysis of ablation flows relative to inertial confinement fusion

Grégoire Varillon[a,b], Jean-Marie Clarisse[a], Arnaud Couairon[b]

a. CEA, DAM, DIF, F-91297 Arpajon, France, jean-marie.clarisse@cea.fr
b. CPHT, CNRS, École polytechnique, IP Paris, F-91128 Palaiseau, France, gregoire.varillon@polytechnique.edu, arnaud.couairon@polytechnique.edu

Résumé :

The hydrodynamic stability of ablation flows is a key issue in laser-driven inertial confinement fusion (ICF) where a sufficiently symmetric implosion of a spherical pellet is expected to achieve thermonuclear burn. Such flows which originate from exposing the pellet outer shell to a growing incident heat flux, present the radial structure of an inward-propagating deflagration, or 'ablation', wave where a shock wave precedes a subsonic heat front that coindices with the leading edge of the heated material expansion wave. Inherently unsteady, these flows are compressible, strongly accelerated and highly nonuniform with a steep heat front, owing to the strong nonlinearity of the heat transport and the intense incident heating. These features, in addition to non-trivial boundary conditions at the shell external surface and shock front, are sources of non-modal thermo-acoustics effects [1, 2]. However non-modal instability growth in ablation flows relevant to ICF has never been studied so far. The development of instabilities leading to nonlinear phenomena in ablation flows could result into the loss of symmetry of the implosion and could finally inhibit ignition. Transition mechanisms in ablation flows are therefore of primary importance to ICF ignition.

Here we investigate non-modal effects in planar radiative ablation waves by using self-similar ablation solutions to the Euler equations with nonlinear heat conduction, without further approximation, as model base flows representative of the early stage of an ICF pellet implosion [3]. Pseudo-spectra of the local approximation of the perturbation evolution operator reveal a potential for strong transient growth. Because of the base flow unsteadiness, our non-modal linear stability analysis relies on a direct-adjoint method. The flow boundary deformations, at the material external surface and shock front, as well as their adjoint variable counterparts enter this method formulation. Both optimal initial conditions and receptivity to perturbations of the incident heat flux and external surface pressure are considered. Different definitions of objective functionals are investigated, some in relation with experimentally measurable quantities. Optimal response computations are carried out for terminal times and perturbation transverse wavelengths which are determined on the basis of pellet implosion features. Computed optimal responses are physically analysed in terms of diffusion and propagation, with the help of a decomposition into linear hyperbolic waves — corresponding to acoustic, entropy, vorticity and radiation-conductivity waves [3] — for a nonuniform heat-conducting flow.

Abstract :

A non-modal linear hydrodynamic stability analysis of ablation waves is carried out for the first time. This analysis is performed for unsteady self-similar solutions in slab symmetry of the Euler equations with nonlinear heat conduction, using a direct-adjoint method that results from a Lagrangian-based optimization problem. Such solutions are considered in connection with inertial confinement fusion (ICF) experiments where the hydrodynamic stability of ablative flows has been identified as a key issue to the achievement of thermonuclear burn. Inherently unsteady, these flows are compressible, highly nonuniform with a steep heat front, and bounded by a material surface and a shock front — features that are possible sources of non-modal thermo-acoustics effects. Non-modal effects are presently exhibited on a particular ablation wave solution. This finding raises the question of the existence and consequences of such effects in configurations of X-ray driven ablation that are more representative of ICF experiments, which is the object of an ongoing investigation.

Mots clefs : écoulement d'ablation, fusion par confinement inertiel, compressible, conduction non-linéaire de chaleur, effets non-normaux, méthode direct adjoint, perturbations optimales

1 Introduction

The hydrodynamic stability of laser-driven ablation flows is a key issue in inertial confinement fusion (ICF) where a sufficiently symmetric implosion of a spherical pellet is expected to achieve thermonuclear burn. Such flows which originate from exposing the pellet outer shell to a growing incident heat flux, present the radial structure of an inward-propagating deflagration, or 'ablation', wave: a shock front precedes a subsonic heat front that coincides with the leading edge of the heated material expansion wave [4, chap. 2] [5, vol. 2, chap. 10, §8]. Inherently unsteady, these flows are compressible, strongly accelerated and highly nonuniform with a steep heat front, owing to the strong nonlinearity of the heat transport and the intense incident heating.

At the early stage of an ICF implosion, the hot outer part of the shell is accelerated toward inner colder and denser layers while the forerunning shock front propagates inward through the shell. This 'shock transit phase' is favourable to ablative Richtmyer–Meshkov and ablative Rayleigh–Taylor instabilities [4, chap. 8],[6]. Hydrodynamic instabilities emerging during this phase seed the subsequent stages of the pellet implosion with perturbations. In particular, perturbations seeded at the start of the acceleration phase of an implosion undergo severe growth, as shown by many studies on the subject, possibly leading to unacceptable loss of symmetry and a failure to achieve the condition of thermonuclear burn. The understanding of hydrodynamic perturbation dynamics during the shock transit phase is therefore of primary importance to ICF.

Perturbations may arise from various sources: external pressure or heat flux inhomogeneities, outer surface defects, inhomogeneities inside the shell or roughness at the shell-fuel interface. Due to this multiplicity, experiments and multiple–physics simulations are often focused on

isolating a particular perturbation (i.e. outer surface roughness) for a single pattern (e.g. Legendre mode). In such cases simulations have been found to be in good agreement with experiments [7, 8]. However this way of proceeding gives poor results when dealing with 'native roughness' targets [7, 9]. Indeed, in such cases, in which no perturbation initially dominates the others, the isolated mode approach fails to render perturbation growth originating from interaction between different perturbation modes. Furthermore, such growth may occur despite the fact that each of these interacting modes could be decaying in time. Perturbation amplification computations can describe such growth provided that they are started from appropriate initial conditions. However it is not feasible to compute the amplification of a sufficiently large set of eligible initial conditions in order to identify which of them lead to an amplification, and, above all, to the *maximum amplification*. As formalized in [10], the information driving the short time evolution of a dynamical system must be searched in the eigenfunctions of its linearized evolution operator rather than merely in this operator eigenvalues which may only be indicative of the system long time behaviour. The set of method and tools for obtaining this information is known as non-modal ananlysis and has been successfully applied to many linear and nonlinear problems in the field of hydrodynamic stability (see [11] and references therein). Non-modal analysis enables the study of these eigenfunctions and the identification of optimal perturbations leading to the maximum amplification at a given time, or optimal boundary conditions when dealing with a receptivity problem. Non-modal analysis has never been applied to the hydrodynamic stability of ablation flows and the present work aims at changing this fact.

We first (§ 2) present the ablation wave modeling that we are using before introducing base flow and linear perturbation equations. An adjoint problem is then established (§ 3) from the Lagrangian based formulation of a linear perturbation optimization problem. This adjoint problem allows us to set up a direct-adjoint looping procedure in order to reach an optimal inital condition maximizing a functional depending on perturbations. Such a procedure is applied to a particular case of ablation flow (§ 4), exhibiting non-modal effects. These results are finally discussed (§ 5), together with perspectives for radiation driven ablation flows.

2 Model

Classically in ICF, hydrodynamic instabilities have been investigated either by multiple-physics simulations, either by modal stability analyses of idealized ablation flows (i.e. steady, quasi-isobaric, discontinuous, etc.) [12]. An alternative to these two opposite approaches uses self-similar solutions to the Euler equations with nonlinear heat conduction as base flows [13, 14, 15]. Such solutions, known since [16], present the advantage of rendering exactly nonuniformity and unsteadiness of ablation waves, and have been exploited to model ICF-type ablation flows [17, 18, 3]. Indeed these self-similar flows present the essential characteristics of an ablation wave, namely: (a) a leading shock front, (b) a quasi-isentropic compression ('post-shock') region, (c) an ablation layer and (d) an expansion wave where heat-condution dominates (the 'conduction region'). The present non-modal stability analysis is based on these self-similar solutions which are in slab symmetry. This slab approximation is reasonable insofar as the shock transit phase corresponds to the beginning of a target implosion: curvature effects for sufficiently small perturbation transverse wavelengths and convergence effects are actually negligible.

2.1 Governing equations

We consider the motion of a polytropic gas in a semi infinite slab subject to an irradiation flux and material pressure at its external boundary. The external irradiation flux is sufficiently high so that nonlinear heat conduction dominates any other diffusive effect (e.g. viscosity). However the fluid temperature is sufficiently low for radiation pressure and radiation energy to be negligible compared to material pressure and internal energy. The material is considered at local thermodynamic equilibrium, allowing us to use a fluid model to describe its motion. Assuming that this motion is along the x direction of Cartesian system of coordinates (O, x, y, z), the equation of motion are written, in dimensionless form and in the Lagrangian coordinate m, where $\mathrm{d}m = \rho \mathrm{d}x$, as [18]

$$\begin{cases} \partial_t 1/\rho - \partial_m v = 0, \\ \partial_t v + \partial_m p = 0, \\ \partial_t (e + v^2/2) + \partial_m (pv + \varphi) = 0, \end{cases} \tag{1}$$

where ρ, v, p , e denote, respectively, the fluid density, velocity, pressure and specific internal energy, and the heat flux is related to the fluid density and temperature T through the expression

$$\varphi = -\rho^{\mathrm{m}} T^{\mathrm{n}} \rho \partial_m T \equiv \Psi(\rho, T, \partial_x T), \quad \mathrm{m} \leq 0, \quad \mathrm{n} > 0. \tag{2}$$

This system is closed by the dimensionless equation of state

$$p = \rho T,$$
$$e = \frac{T}{\gamma - 1}, \text{ with } \gamma \text{ the adiabatic gas exponent.}$$

Self-similar reductions of (1) arise if the incident heat flux and pressure at the external surface follow specific power laws [16, 13], namely

$$\varphi(0,t) = \mathcal{B}_\phi t^{3\alpha-3}\ ,\ p(0,t) = \mathcal{B}_p t^{2\alpha-2}, \text{ for } t > 0, \text{ with } \alpha = \frac{2\mathrm{n}-1}{2\mathrm{n}-2}\,, \tag{3}$$

and for an initial state given by $(\rho, v, T) = (1, 0, 0)$ for $m \geq 0$. For certain values of the boundary parameters $(\mathcal{B}_p, \mathcal{B}_\varphi)$, such solutions present the features of an ablation wave extending from the flow external surface $(m = 0)$ through an ablation front up to the fore-running shock front [3, 18]. In particular, all the peculiarities of an ablation wave driven by a nonlinear heat conduction are described in a smooth manner, without any further approximation, including the temperature and density stratification of the conduction region. In the present case, highly accurate solutions to (1), (3) are obtained by means of an adaptive multidomain Chebyshev spectral method [20].

2.2 Linear perturbations

Three-dimensional linear perturbations of the above self-similar ablative waves are considered using an Eulerian description in the coordinate system (m, y, z). The resulting system of partial differential equations in physical space is replaced by a one-dimensional system in the yz-Fourier space. With the notation $\widehat{f}$ for the yz-Fourier component of the base flow quantity

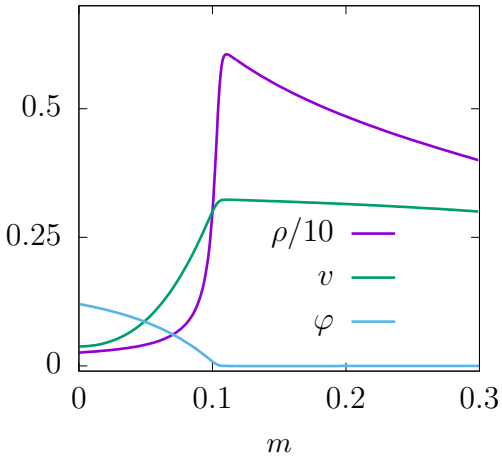

Figure 1: Self-similar ablation wave for the electron heat conduction model of Spitzer [19] ($\mathrm{m}=0, \mathrm{n}=5/2$) and boundary condition parameters $(\mathcal{B}_p, \mathcal{B}_\phi) = (0.124, 0.120)$ of (1). Spatial profiles in the coordinate m at time $t_0 = 1$ of the fluid density ρ, longitudinal velocity v and heat flux φ.

f with transverse wavenumber $k_\perp = \sqrt{k_x^2 + k_y^2}$, this system reads

$$\partial_t \widehat{U} = L\widehat{U} \equiv -\boldsymbol{A}\partial^2_{m^2}\widehat{U} - \boldsymbol{B}\partial_m \widehat{U} - \boldsymbol{C}\widehat{U}\ , \tag{4}$$

with $\widehat{U} = \left[\widehat{\rho}\,\widehat{v}\,\widehat{d}_\perp\,\widehat{T}\right]^\top$, where $\widehat{d}_\perp$ denotes the Fourier component of the transverse divergence of the transverse velocity, and with the matrices $\boldsymbol{A}$, $\boldsymbol{B}$ and $\boldsymbol{C}$ defined by

$$\boldsymbol{A} = \begin{pmatrix} 0 & 0 & 0 & 0 \\ 0 & 0 & 0 & 0 \\ 0 & 0 & 0 & 0 \\ 0 & 0 & 0 & C_v^{-1}\,\rho\,\Psi_{T'} \end{pmatrix},\ \boldsymbol{B} = \begin{pmatrix} 0 & \rho^2 & 0 & 0 \\ T & 0 & 0 & \rho \\ 0 & 0 & 0 & 0 \\ C_v^{-1}\,\Psi_\rho & C_v^{-1}\,p & 0 & B_{44} \end{pmatrix},$$

$$\boldsymbol{C} = \begin{pmatrix} \rho\partial_m v & \rho\partial_m \rho & \rho & 0 \\ T\partial_m\rho/\rho & \rho\partial_m v & 0 & \partial_m\rho \\ k_\perp^2 T/\rho & 0 & 0 & -k_\perp^2 \\ C_{41} & \rho\partial_m T' & C_v^{-1}\,T & C_{44} \end{pmatrix},$$

$$B_{44} = C_v^{-1}\left[\partial_m(\rho\Psi_{T'}) + \Psi_T\right], \quad C_{41} = C_v^{-1}\left(\partial_m\Psi_\rho - \rho^{-1}\,\partial_m\varphi\right),$$
$$C_{44} = C_v^{-1}\left[\rho\partial_m v + \partial_m\Psi_T - k_\perp^2\rho^{-1}\,\Psi_{T'}\right].$$

The longitudinal perturbation of the heat flux expands as $\widehat{\varphi}_x = \widehat{\rho}\,\Psi_\rho + \widehat{T}\,\Psi_T + \rho\Psi_{T'}\partial_m\widehat{T}$ where Ψ_ρ, Ψ_T and $\Psi_{T'}$ stands for the partial derivatives of Ψ (2) with respect to the density, the temperature and the temperature gradient. Similarly, the transverse perturbation of the heat flux expands as $\nabla_\perp \cdot \widehat{\boldsymbol{\varphi}}_\perp = k_\perp^2\,\Psi_{T'}\,\widehat{T}$.

The external surface and shock front are also perturbed and their linear deformations are denoted $\widehat{X}_{\mathrm{ext}}(t)$ and $\widehat{X}_{\mathrm{sf}}(t)$, respectively. Perturbed boundary conditions arise from a first order expansion of (3) [14] between the mean position of the boundary surface and its perturbed

position. At the external surface, perturbations in density and heat flux are imposed:

$$\widehat{\rho}_{\text{ext}}(t) = \widehat{\rho}(0,t) + \widehat{X}_{\text{ext}}(t)\rho(0,t)\partial_m\rho|_{m=0}\,, \tag{5a}$$

$$\widehat{\varphi}_{\text{ext}}(t) = \widehat{\varphi}(0,t) + \widehat{X}_{\text{ext}}(t)\rho(0,t)\partial_m\varphi|_{m=0}\,, \tag{5b}$$

and the following kinematic relation at this material surface applies

$$\widehat{v}_{\text{ext}}(t) = \dot{\widehat{X}}_{\text{ext}}(t) = v(0,t) + \widehat{X}_{\text{ext}}(t)\rho(0,t)\partial_m v|_{m=0} \tag{5c}$$

At the shock front, Rankine–Hugoniot relations are perturbed to the first order and take the form of four linear equations relating flow perturbations at the shock front, to shock front deformation $\widehat{X}_{\text{sf}}$, shock front deformation velocity $\dot{\widehat{X}}_{\text{sf}}$, and to the upstream state perturbation, say

$$RH\left(\widehat{U}_{\text{sf}-}, \widehat{X}_{\text{sf}}, \dot{\widehat{X}}_{\text{sf}}, \widehat{U}_{\text{sf}+}\right) = 0. \tag{6}$$

System (4) is composed of a parabolic scalar subequation stemming from the total energy conservation, and a hyperbolic subsystem corresponding to the equations of isothermal gas dynamics. Therefore (4) is incompletely parabolic [21] and the problem (4)-(6) is well-posed if at each boundary: one boundary condition is applied on the parabolic subequation and one boundary condition is applied on each of the incoming waves of the hyperbolic subsystem. For $a =$'ext' and 'sf', boundary condition operators are formalized as

$$BC_a^h\left(\widehat{U}|_a, \widehat{X}_a\right) = 0,$$
$$BC_a^p\left(\widehat{U}|_a, \widehat{X}_a\right) = 0,$$

where BC_a^p is a scalar operator and the dimension of BC_a^h equals the number of incoming waves at the given boundary.

3 Optimal perturbations through a Lagrangian

In the present work we are interested in finding the initial states $\{\widehat{U}(t_0,m), \widehat{X}_{\text{ext}}(t_0), \widehat{X}_{\text{sf}}(t_0)\}$ maximizing an objective functional $\mathcal{J}$ depending only on the final state $\{\widehat{U}(T,m), \widehat{X}_{\text{ext}}(T), \widehat{X}_{\text{sf}}(T)\}$, where $\{\widehat{U}, \widehat{X}_{\text{ext}}, \widehat{X}_{\text{sf}}\}$ are solutions of (4)-(6) where $\widehat{\rho}_{\text{ext}}$ and $\widehat{\varphi}_{\text{ext}}$ are kept to zero. For this purpose we choose to perform the optimization in an unconstrained space through the definition of a Lagrangian where Lagrange multipliers are introduced to enforce evolution equations, boundary conditions and a constraint on the initial conditions. This Lagrangian reads

$$\begin{aligned}\mathcal{L}(\widehat{U},\, \widehat{X},\, \widehat{U}^\dagger,\, \widehat{\nu}^\dagger,\, \widehat{\eta}^\dagger,\, \widehat{\mu}^\dagger,\, \beta^\dagger) = \\ \mathcal{J} - \int_{m=0,t=t_0}^{m_{\text{sf}},T} \widehat{U}^\dagger\left(\partial_t\widehat{U} - L(\widehat{U})\right)\mathrm{d}t\mathrm{d}m - \int_{t_0}^{T}\widehat{\nu}_a^\dagger BC_a^h\mathrm{d}t \\ - \int_{t_0}^{T}\widehat{\eta}_a^\dagger BC_a^p\mathrm{d}t - \int_{t_0}^{T}\widehat{\mu}_a^\dagger f_a\mathrm{d}t - \beta^\dagger\left(\mathcal{I} - K_0\right),\end{aligned} \tag{7}$$

where subscripts a are summed over boundaries: 'ext' and 'sf'. Scalar quantities f_a stand for the evolution equations of $\widehat{X}_a$, taken from (5) and (6), and K_0 is the normalization constant

Lagrange multiplier	Corresponding constraint
$\widehat{U}^\dagger$	Evolution equation for perturbations
$\widehat{\nu}^\dagger_{\text{ext}}$ and $\widehat{\nu}^\dagger_{\text{sf}}$	Hyperbolic boundary conditions at the external surface and shock front
$\widehat{\eta}^\dagger_{\text{ext}}$ and $\widehat{\eta}^\dagger_{\text{sf}}$	Parabolic boundary condition at the external condition and shock front
$\widehat{\mu}^\dagger_{\text{ext}}$ and $\widehat{\mu}^\dagger_{\text{sf}}$	Evolution equation for boundary deformations
$\beta^\dagger$	Normalization of the initial condition

Table 1: Lagrange multipliers used in (7).

for initial conditions. Lagrange multipliers used in (7) are defined in Tab. 1.

The normalization functional $\mathcal{I}$ depends only on the initial state t_0 and may differ from the objective functional $\mathcal{J}$. The optimum lies in the stationary points of the Lagrangian [22]. Differentiating with respect to the state variables leads to the adjoint problem

$$\partial_t \widehat{U}^\dagger = L^\dagger \widehat{U}^\dagger \equiv \boldsymbol{A}^\top \partial_m^2 \widehat{U}^\dagger + (2\,\partial_m \boldsymbol{A} - \boldsymbol{B})^\top \partial_m \widehat{U}^\dagger + (\partial_m^2 \boldsymbol{A} - \partial_m \boldsymbol{B} + \boldsymbol{C})^\top \widehat{U}^\dagger, \tag{8a}$$

$$BC_a^{h\,\dagger} = 0, \quad BC_a^{p^\dagger} = 0, \tag{8b}$$

$$\mathrm{d}_t \widehat{X}_a^\dagger = \dot{\widehat{X}}_a^\dagger, \tag{8c}$$

where $\dot{\widehat{X}}_a^{\ \dagger}$ and $\widehat{X}_a^\dagger$ are scalar linear combinations of $\widehat{\nu}_a^\dagger$, $\widehat{\eta}_a^\dagger$ and $\widehat{\mu}_a^\dagger$. The adjoint problem (8a) is to be integrated backward in time, from a terminal condition, to be well posed. The terminal condition reads

$$\widehat{U}^\dagger(T, m) = \nabla_{\widehat{U}|_T} \mathcal{J}, \tag{9a}$$

$$\widehat{X}_a^\dagger(T) = \nabla_{\widehat{X}_a|_T} \mathcal{J}. \tag{9b}$$

Differentiating with respect to the control parameter, $\widehat{U}(t_0, m), \widehat{X}_a(t_0)$, gives the optimality conditions. Away from an optimum we have

$$\nabla_{\widehat{U}|_{t_0}} \mathcal{L} = \widehat{U}^\dagger|_{t_0} - \beta^\dagger \nabla_{\widehat{U}|_{t_0}} \mathcal{I}, \tag{10a}$$

$$\nabla_{\widehat{X}_a|_{t_0}} \mathcal{L} = \widehat{X}_a^\dagger|_{t_0} - \beta^\dagger \nabla_{\widehat{X}_a|_{t_0}} \mathcal{I}. \tag{10b}$$

At an optimum, the right-hand-sides in (10) vanish. Solving (4) and (8), along with (5) and (10), simultaneously would require a global approximation over the time interval, resulting in a resource intensive procedure. Classically, direct and adjoint problems are solved iteratively, using forward and backward temporal integrations, from a given starting initial condition. Successive initial conditions of the direct problem are found thanks to an iterate power method [23] or a relaxation method [24]. Both methods give similar results. Numerical solutions to the direct system (4)-(6) and to the adjoint system (8), with proper initial conditions, are obtained, in the variable m, using the same multidomain pseudospectral method as for the base flow and, in time, with a three-step implicit-explicit Runge–Kutta scheme. Boundary conditions are handled using a penalty method while matching conditions at subdomain interfaces are enforced exactly. The numerical codes for the direct and adjoint problems perform computations over

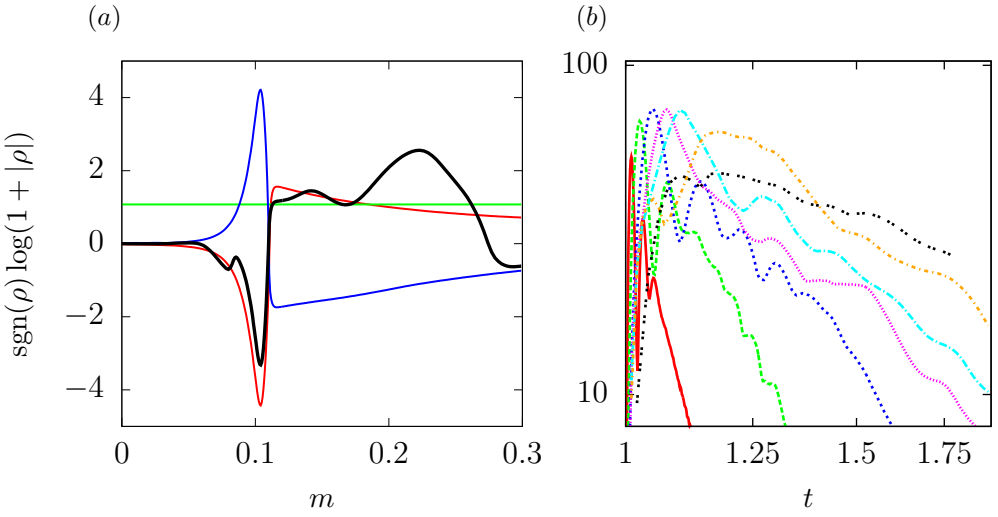

Figure 2: (a) Density perturbation profiles of the starting initial conditions given by (thick lines): a translation of the base flow (red), a uniform perturbed state (green) and a perturbed state resulting from a previous external heat flux perturbation (blue). Common optimal initial density profile (thick black line) for a final time $T = 2$. (b) Objective functional for final times $T = 1.01$, 1.025, 1.05, 1.075, 1.1, 1.2 and 1.6, from bottom to top, for $k_\perp = 0.1$.

each subdomain in parallel using the MPI paradigm with a single process per subdomain.

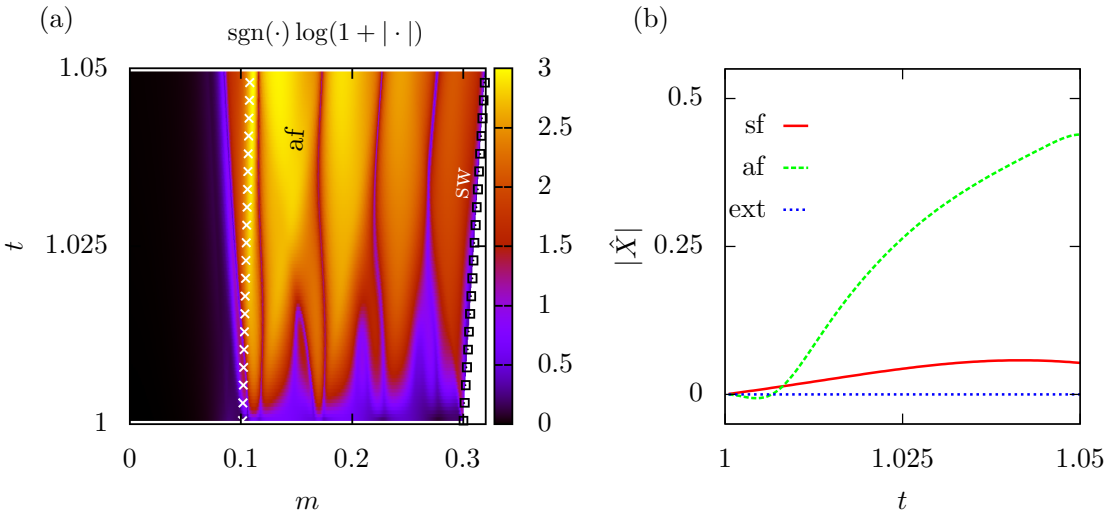

Figure 3: (a) Intensity map in the variables (m, t) of the local Euclidean norm of the solution to (4) with optimal initial condition for final time $T = 1.05$ and $k_\perp = 0.1$. (b) Time evolution of the deformations of the external surface (blue), the ablation front (green) and the shock front (red).

4 Optimal perturbation of a particular ablation flow

We consider the case of an ablation flow resulting from the direct illumination of the target by a laser. In that case the irradiation flux corresponds to the laser light, propagating in the expanding material up to the critical surface where the density exceeds a critical value. This critical surface corresponds, in our model, to the external surface of the ablation flow where the

laser energy is deposited and a material pressure is applied. Heat is transported *via* electron heat conduction [5, chap. VII, §12]. Base flow profiles are shown on Fig. 1. The ablation front is defined as the location of the temperature gradient length minimum. The latter defines the characteristic length of the ablation front, $l_{\rm af}(t)$. The conduction region, of length $l_{\rm cond}(t)$, extends from the external surface ($m = 0$) up to the ablation front ($m_{\rm af} = 0.1013$), and the quasi-isentropic post-shock region extends from the ablation layer up to the shock front ($m_{\rm sf} = 0.3$). Lengths scale as $l(t) = t^\alpha\, L$ due to self-similarity, where L is a reduced length (Tab. 2).

max M	0.37
$M\|_{\rm af}$	0.13
$Fr\|_{\rm af}$	2.07
$L_{\rm cond}$	$1.013\,10^{-1}$
$L_T/L_{\rm tot}$	$2.66\,10^{-2}$

Table 2: Main characteristics of the ablation flow of Fig. 1: maximum of the flow Mach number relative to the ablation front, max M, ablation front value of this Mach number, $M|_{\rm af}$, and of the Froude number, $Fr|_{\rm af}$, heat conduction region reduced length, $L_{\rm cond}$, and ratio of the reduced ablation front characteristic length L_T to the ablation wave reduced length $L_{\rm tot}$ (defined in [3]).

Computations have been carried out for various transverse wavenumbers and we present here the results for $k_\perp = 0.1$. The objective functional is chosen as the L_2 norm of state variables, namely

$$\mathcal{J} = \frac{1}{2}\int_0^{m_{\rm sf}} \widehat{U}^2(T,m)\mathrm{d}m + \frac{1}{2}\left(\widehat{X}^2_{\rm ext}(T) + \widehat{X}^2_{\rm sf}(T)\right). \tag{11}$$

The convexity of this functional with respect to our set of control parameter is not established. However a numerical experiment shows that initiating the optimization procedure with three different initial conditions leads to the same optimal condition (Fig. 2a). Computations are carried out on a 20 domain grid, each domain containing 50 collocation points. An iteration is composed of the integration of (4) from t_0 to T and (8a) backward, and requires $7\,10^5$ time steps for $T = 4$. Convergence is reached when the L_2 norm of the difference between two successive initial conditions is below a defined threshold (10^{-5}). Reaching convergence requires between 20 and 30 iterations depending on the final time.

At first, optimal initial conditions are obtained for final times ranging from 1.01 to 1.6. The envelope of their L_2 norm across time shows that maximum amplification occurs at $T = 1.05$ (Fig. 2b). It has been observed that perturbations behave like travelling waves, here termed pseudo-characteristic waves, with reflection and coupling at the external surface, the shock front and in the ablation layer. Such pseudo-characteristic waves have been found appropriate for describing perturbations propagating in the conduction region and the post-shock region of ablation flows [3, 25] and their nature is recalled in Tab. 3. Optimal initial conditions and their evolution up to the optimal time are analysed by characterizing them in terms of these longitudinal pseudo-characteristic waves.

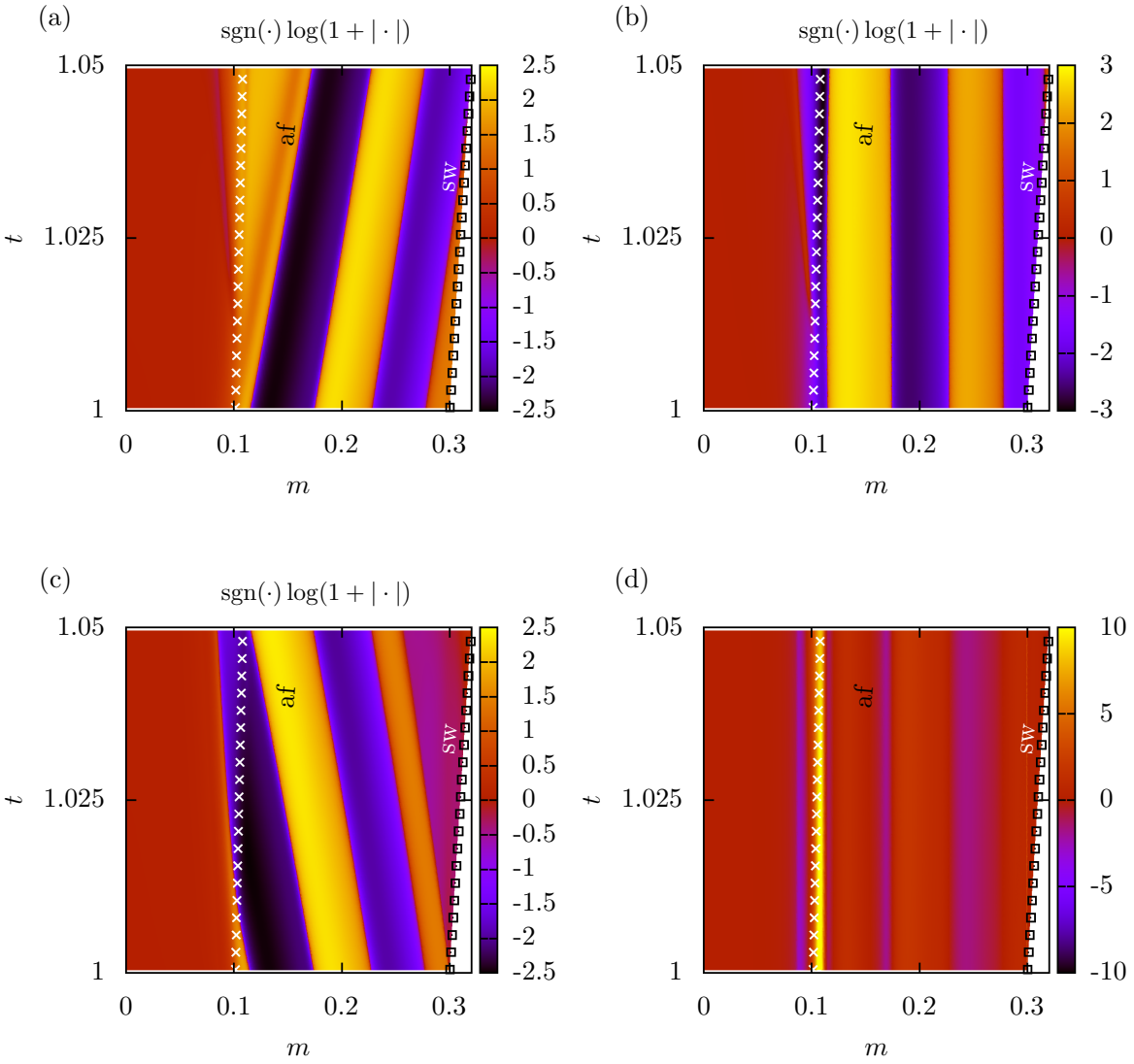

Figure 4: Projection on pseudo-characteristic variables defined in Tab. 3 of the solution to (4), for $T = 1.05$ and $k_\perp = 0.1$, in the variables (m, t): (a) $\widehat{\mathcal{W}}_1$, (b) $\widehat{\mathcal{W}}_2$, (c) $\widehat{\mathcal{W}}_3$ and (d) $\widehat{\omega}/\rho$.

Maximum amplification The optimal initial condition realizing the maximum amplification, at $T = 1.05$, is projected onto the pseudo-characteristic waves described in Tab. 3. This initial condition is very weak in the conduction region, presents a peak in the ablation layer and two oscillations over the post-shock region corresponding to: in phase upstream and downstream propagating acoustic waves, and, in opposite phase, an entropy wave (Fig. 4). Perturbations mainly evolve in the post-shock region and the ablation layer (Fig. 3a). Indeed, the final time is too short, relatively to propagation velocities, for a significant propagation of perturbations. As a result the external surface remains unperturbed while the ablation front and the shock front undergo distortions (Fig. 3b). Moreover, heat diffusion is negligible in the post-shock region and its effects in the ablation layer is much weaker than wave couplings. The present transient growth is therefore mainly due to local constructive interactions between pseudo-characteristic waves (Fig. 4) rather than interactions between the different regions of the flow through such waves. Maximum amplification occurs while the upstream, downstream

Wave	*conduction region*	*post-shock region*
$\widehat{\mathcal{W}}_1$	Heat conductivity	quasi-isentropic acoustic
$\widehat{\mathcal{W}}_2$	quasi-isothermal acoustic	quasi-entropy
$\widehat{\mathcal{W}}_3$	Downstream quasi-isothermal acoustic	Downstream quasi-isentropic acoustic
$\widehat{\omega}/\rho$	Vorticity	Vorticity

Table 3: Definition of the pseudo-characteristic waves used for analysing flow perturbations.

acoustic and entropy waves are superimposed and in phase (Fig. 4a, b and c), in addition to the arrival of the main contribution of vorticity at the ablation front (Fig. 4d).

As noted, maximum amplification occurs at a final time, $T = 1.05$, for which only local effects act and non-local effects do not have time to develop. However, the shock transit phase of an actual ICF target may last much longer than this maximum amplification time. Indeed, during this phase, the external surface, ablation front and shock front may interact several times *via* travelling waves and heat diffusion across the conduction and post-shock regions. Hence, non-local effects should arise in addition to local interactions and it is of interest to determine the optimal initial condition for such a regime.

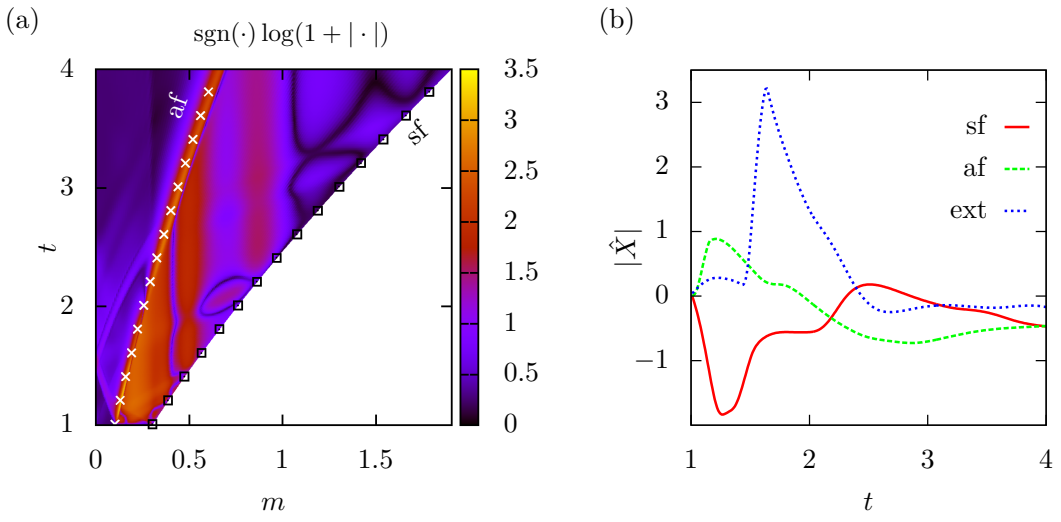

Figure 5: Intensity map in the variables (m, t) of the local Euclidean norm of the solution to (4) with optimal initial condition for final time $T = 4$ and $k_\perp = 0.1$. (b) Time evolution of the deformations of the external surface (blue), the ablation front (green) and the shock front (red).

Amplification at the time horizon of the shock transit phase The terminal time is chosen to be consistent with the duration of a shock transit phase. Simulations have shown that during this phase a few interactions between the shock front and the ablation front occur through acoustic and entropy/vorticity waves. Here, the value of $T = 4$ satifies this condition (Fig. 6a, b and c). As for the maximum amplification case, the present optimal initial condition displays higher levels in the post-shock region than in the conduction region although initial perturbations in this region are no longer negligible. The same arrangement of acoustic and

entropy waves is observed in the post-shock region but over a single spatial lobe. In the conduction region, the optimal initial condition is dominated by acoustic waves. External surface and shock front deformations undergo strong transient growth each time travelling waves interact with them, before relaxing to lower absolute values (Fig. 5b). At the final time, much of the contribution to the functional $\mathcal{J}$ lies in the ablation layer and in the entropy perturbations that propagate in the post-shock region (Fig. 5a). Regarding interfaces, most of the contribution comes front the shock front deformation rather than the external surface deformation. We note that the optimal response for $T = 4$ reaches a maximum at a smaller time than the terminal time. The amplification of the ablation front deformation relatively to its initial value is $2.2\,10^2$ at its maximum and $1.1\,10^2$ at the final time. Such final time amplification indicates that the ablation front could remain strongly deformed at the end of the shock transit phase. This would bring a significant seed for ablative Rayleigh–Taylor instabilities to develop during a subsequent acceleration stage of an ICF implosion.

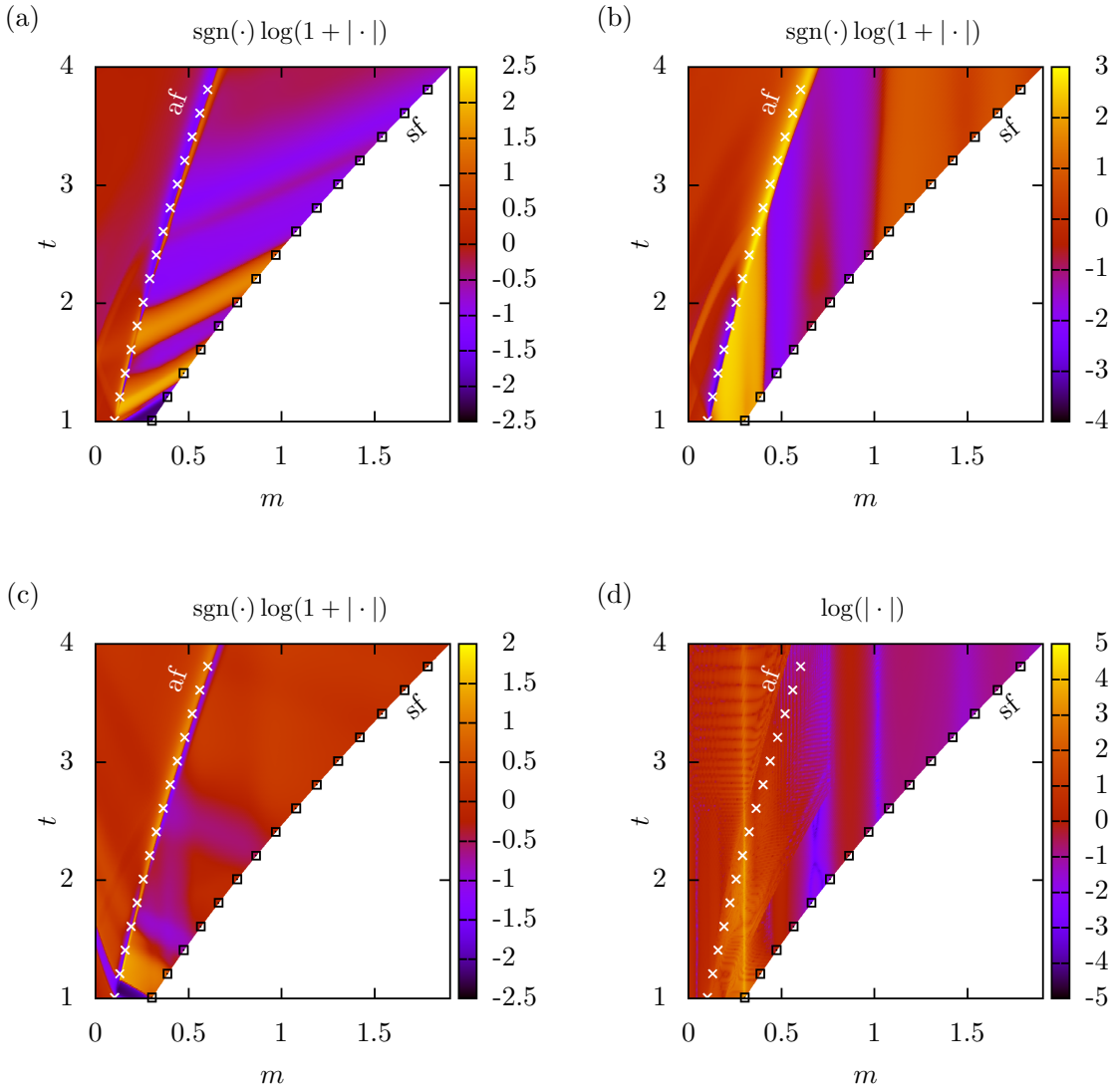

Figure 6: Projection on pseudo-characteristic variables defined in Tab. 3 of the solution to (4), for $T = 4$ and $k_\perp = 0.1$, in the variables (m, t): (a) $\widehat{\mathcal{W}}_1$, (b) $\widehat{\mathcal{W}}_2$, (c) $\widehat{\mathcal{W}}_3$ and (d) $\widehat{\omega}/\rho$.

5 Discussion and conclusion

In the present work, we carry out the first non-modal stability analysis of an ablation flow. These flows are compressible, non uniform, non stationary and present steep gradients, owing to nonlinear heat conduction, and moving boundaries. A Lagrangian based formulation of the optimization of linear perturbations and boundary deformations is devised. Optimal initial conditions are computed thanks to a direct-adjoint looping. This method is applied to a particular configuration for which we have exhibited significant transient growth for various time horizons. These results prove the existence of non-modal effects in ablation waves, which may be of concern to ICF experiments. They entice us to carry out a systematic non-modal analysis of ICF-like ablation flows driven by X-ray irradiation.

Optimal perturbation computations of radiation driven ablation flows presenting characteristic features of ICF target implosions are ongoing, but they are numerically more demanding. Indeed, such flows present much steeper ablation fronts: as a comparison, their ratio of characteristic lengths (see Tab. 2) range from 10^{-3} to 10^{-5}. This necessarily leads to refined meshes and smaller time steps. As a result, between 10^6 to 10^8 time steps are required for a single direct-adjoint iteration. We believe that, similarly to electron heat conduction results presented in this paper, convergence would be reached within 20 to 30 iterations.

We also expect to find similar local interactions for short-time optimal initial conditions, and non local interactions for optimal initial conditions corresponding to shock transit times of radiation driven ablation flows. Various objective functionals will be tested, corresponding to energy norms (i.e. acoustic, rotational or total energy) or observables (i.e. optical depth or ablation front deformations).

References

[1] K. Wieczorek, C. Sensiau, W. Polifke, and F. Nicoud. Assessing non-normal effects in thermoacoustic systems with mean flow. *Phys. Fluids*, 23, 2011.

[2] F. Nicoud, L. Benoit, C. Sensiau, and T. Poinsot. Acoustic modes in combustors with complex impedances and multidimensional active flames. *AIAA Journal, American Institute of Aeronautics and Astronautics*, 45(2):426–441, 2007.

[3] J.-M. Clarisse, J.-L. Pfister, S. Gauthier, and C Boudesocque-Dubois. A hydrodynamic analysis of self-similar radiative ablation flows. *J. Fluid Mech.*, 848:219–255, 2018.

[4] S. Atzeni and J. Meyer-ter-Vehn. *The physics of inertial fusion.* Oxford University Press, Oxford, U.K., 2004.

[5] Ya. B. Zel'dovich and Yu. P. Raizer. *Physics of shock waves and high-temperature hydrodynamic phenomena.* Academic Press, New-York, 1967.

[6] Y. Aglitskiy, A. L. Velikovich, M. Karasik, N. Metzler, S. T. Zalesak, A. J. Schmitt, L. Phillips, J. H. Gardner, V. Serlin, J. L. Weaver, and S. P. Obenschain. Basic hyrdodynamics of Richtmyer–Meshkov-type growth and oscillations in the inertial confinement fusion-relevant conditions. *Phil. Trans. R. Soc. A*, 368:1739–1768, 2010.

[7] K. S. Raman et al. An in flight radiography platform to measure hydrodynamic instability growth in inertial confinement fusion capsules at the national ignition facility. *Phys. Plasmas*, 21, 2014.

[8] J. L. Peterson, D. T. Casey, O. A. Hurricane, K.S. Raman, H.F. Robey, and V.A. Smalyuk. Validating hydrodynamic growth in national ignition facility implosions. *Phys. Plasmas*, 22, 2015.

[9] V. A. Smalyuk, S. V. Weber, D. T. Casey, D. S. Clark, J. E. Field, S. W. Haan, B. A. Hammel, A. V. Hamza, D. E. Hoover, O. L. Landen, A. Nikroo, H. F. Robey, and C. R. Weber. Hydrodynamic instability growth of three-dimensional, "native-roughness" modulations in x-ray driven, spherical implosions at the National Ignition Facility. *Phys. Plasmas*, 22:072704, 2015.

[10] L. N. Trefethen, A. E. Trefethen, S. C. Reddy, and T. A. Driscoll. Hydrodynamic stability without eigenvalues. *Science*, 261:578–584, 1993.

[11] P. Luchini and A. Bottaro. Adjoint equations in stability analysis. *Annu. Rev. Fluid Mech.*, 46(1):493–517, 2014.

[12] V. Bychkov, M. Modestov, and C. K. Law. Combustion phenomena in modern physics: I. Inertial confinement fusion. *Prog. Energy Combust. Sci.*, 47:32–59, 2015.

[13] F. Abéguilé, C. Boudesocque-Dubois, J.-M. Clarisse, S. Gauthier, and Y. Saillard. Linear perturbation amplification in self-similar ablation flows of inertial confinement fusion. *Phys. Rev. Lett.*, 97:035002, 2006.

[14] J.-M. Clarisse, C. Boudesocque-Dubois, and S. Gauthier. Linear perturbation response of self-similar ablative flows relevant to inertial confinement fusion. *J. Fluid Mech.*, 609:1–48, 2008.

[15] V. Lombard, S. Gauthier, J.-M. Clarisse, and C. Boudesocque-Dubois. Kovásznay modes in stability of self-similar ablation flows of ICF. *Europhys. Lett.*, 84:25001, 2008.

[16] R. Marshak. Effect of radiation on shock wave behavior. *Phys. Fluids*, 1(1):24–29, 1958.

[17] J. Sanz, A. R. Piriz, and F. G. Tomasel. Self-similar model for tamped ablation driven by thermal radiation. *Phys. Fluids B*, 4(3):683–692, 1992.

[18] C. Boudesocque-Dubois, S. Gauthier, and J.-M. Clarisse. Self-similar solutions of unsteady ablation flows in inertial confinement fusion. *J. Fluid Mech.*, 603:151–178, 2008.

[19] J. Duderstadt and G. Moses. *Inertial confinement fusion.* Wiley-Interscience, 1982.

[20] C. Boudesocque-Dubois, V. Lombard, S. Gauthier, and J.-M. Clarisse. An adaptive multidomain Chebyshev method for nonlinear eigenvalue problems: Application to self-similar solutions of gas dynamics equations with nonlinear heat conduction. *J. Comput. Phys.*, 235:723–741, 2013.

[21] J. C. Strikwerda. Initial boundary value problems for incompletely parabolic systems. *Commun. Pure Appl. Math.*, XXX:797–822, 1977.

[22] M. D. Gunzburger. Introduction into mathematical aspect of flow control and optimization. In von Karman Institute for Fluid Dynamics, editor, *Lecture Series 1997-05 on Inverse Design and Optimisation Methods*. April 1997.

[23] P. Corbett and A. Bottaro. Optimal perturbations for boundary layers subject to streamwise pressure gradient. *Phys. Fluids*, 12(1):120–130, 2000.

[24] Y. Duguet, A. Monokrousos, L. Brandt, and D. S. Henningson. Minimal transition thersholds in plane couette flow. *Phys. Fluids*, 25, 2013.

[25] G. Varillon, J.-M. Clarisse, and A. Couairon. Investigation of supersonic heat-conductivity linear waves in ablation flows. In *EPS Plasma Physics Conference*, Prague, Czech Republic, July 2018.